IEEE Photonics Journal
An IEEE Photonics Society Publication

Extreme Miniaturization of Silicon Add–Drop Microring Filters for VLSI Photonics Applications

Volume 2, Number 3, June 2010

Ashok M. Prabhu
Alan Tsay
Zhanghua Han
Vien Van

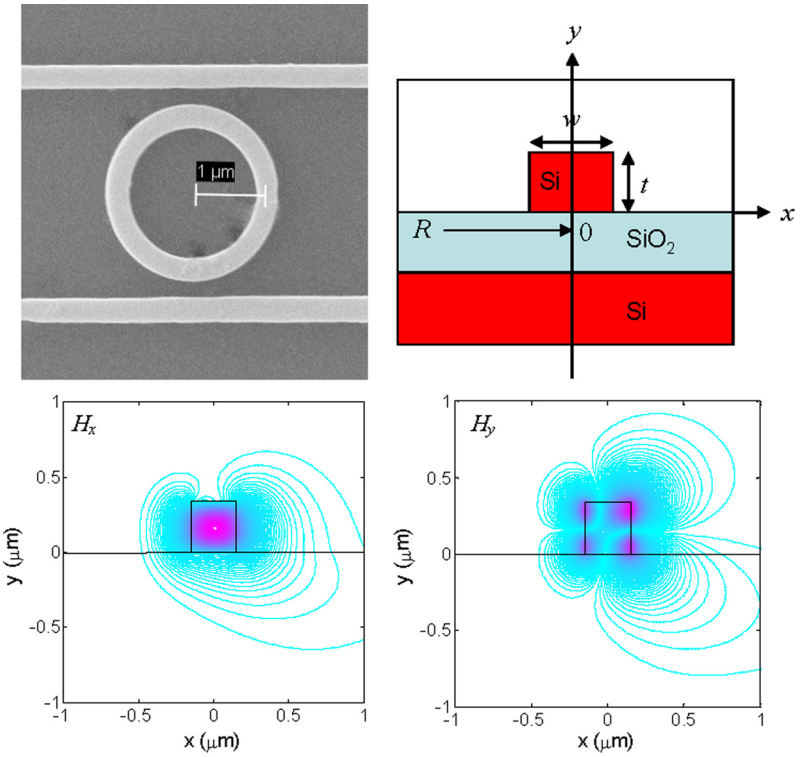

DOI: 10.1109/JPHOT.2010.2049831
1943-0655/$26.00 ©2010 IEEE

Extreme Miniaturization of Silicon Add–Drop Microring Filters for VLSI Photonics Applications

Ashok M. Prabhu, Alan Tsay, Zhanghua Han, and Vien Van

Department of Electrical and Computer Engineering, University of Alberta, Edmonton, AB T6G 2V4, Canada

DOI: 10.1109/JPHOT.2010.2049831
1943-0655/$26.00 ©2010 IEEE

Manuscript received April 1, 2010; revised April 30, 2010; accepted April 30, 2010. Date of publication May 6, 2010; date of current version June 4, 2010. This work was supported in part by the Natural Sciences and Engineering Research Council of Canada. Corresponding author: A. M. Prabhu (e-mail: ashok.prabhu@ualberta.ca).

Abstract: We theoretically and experimentally investigated the performance of silicon-on-insulator (SOI) microring add–drop filters in the limit of extreme miniaturization for potential application in very dense integration of silicon photonic devices. Rigorous numerical analyses were performed to predict the theoretical limit of achievable intrinsic quality factors as the microring radius is scaled down to 1 μm. Experimental measurements of fabricated SOI microring resonators showed that ultracompact add–drop microring filters with radii as small as 1 μm can be achieved with a free spectral range exceeding 80 nm and an insertion loss of only 1 dB. These devices are also shown to exhibit intrinsic quality factors approaching the theoretically achievable limit set by the bending loss in ultracompact microring resonators.

Index Terms: Silicon nanophotonics, VLSI photonics, microring resonators.

1. Introduction

Silicon-on-insulator (SOI) has recently emerged as a promising material system for very large-scale integration (VLSI) of photonic devices due to its high index contrast and compatibility with conventional Complementary Metal–Oxide–Semiconductor (CMOS) fabrication technology. The high index contrast of SOI allows compact photonic elements based on strongly confined silicon wires with submicron dimensions and tight bending radii to be realized. One of the key elements which lends itself to the miniaturization of silicon photonic devices is the microring resonator, whose compact size and versatility can greatly enhance the functionality of VLSI silicon photonic circuits, as demonstrated in a wide range of applications such as wavelength-division-multiplexing (WDM) filters [1], on-chip optical interconnects [2], modulators [3], and optical delay lines [4]. The microring resonators in these reported applications typically have radii in the range of 5–10 μm and can be fabricated to have very low loss, with intrinsic quality factors (Q factors) on the order of 10^5 achievable using CMOS-compatible fabrication processes.

Since the footprint of a microring resonator scales with the square of its radius, there is a strong motivation to minimize the ring radius in order to achieve denser device integration. An added advantage of miniaturization is that the free spectral range (FSR) of the resonator becomes larger, which is desirable for WDM add–drop filters. Although decreasing the microring radius also leads to more pronounced bending loss, we showed in [5] that it is possible to mitigate the effect of extreme

resonator loss by adjusting the external coupling strength in order to achieve a specific add–drop filter performance such as insertion loss and extinction ratio.

Several attempts at miniaturizing silicon microrings have recently been reported in the literature. In [6], a compact SOI microring add–drop resonator with a 2-μm radius was demonstrated with a Q factor of 6730 and an FSR of 47 nm, although the insertion loss of the device was not reported. In [7], an all-pass SOI microring resonator with a 1.5-μm radius was demonstrated, with a reported Q factor of 9000 and a wide FSR of 62.5 nm. However, the transmission (drop-port) characteristic of the device could not be experimentally assessed because of the lack of an output waveguide. Recently, we also reported a compact add–drop filter based on a 1.5-μm-radius SOI microring resonator with a wide bandwidth of 210 GHz, an insertion loss of 3 dB, and a deep extinction of 25 dB [5]. Add–drop microring filters with smaller radii have not been reported.

In this paper, we theoretically and experimentally investigate the potential for extreme miniaturization of silicon add–drop microring filters with ring radii scaled down to around 1 μm. Our objectives are to determine the achievable filter performance and identify the important sources of intrinsic and extrinsic loss in these ultracompact devices. Toward these goals, we performed rigorous numerical analyses of SOI microrings with very small bending radii to determine the theoretical limit on the achievable intrinsic Q factors of these resonators. To experimentally assess the performance of the filters, a set of SOI add–drop microring resonators with radii between 1.5 μm and 1 μm were fabricated using an electron-beam-lithography (EBL)-based fabrication process. These devices represent some of the smallest add–drop microring filters ever realized in any material system, each occupying a footprint of only a few squared microns. Experimental measurements showed that practical add–drop microring filters with insertion loss less than 1 dB can be achieved with ring radii as small as 1 μm. We also found that it is the extrinsic loss due to coupling junction scattering, and not the intrinsic bending loss, that is the dominant source of loss in these ultracompact devices and that our fabricated microring resonators exhibited intrinsic Q factors very close to the theoretically achievable limit set by the bending loss. Although EBL was used in this work as an experimental approach to achieving miniaturization of microring resonators, we note that other, fully CMOS-compatible processes such as those based on Deep Ultraviolet Lithography [8] would provide a more practical approach to realizing low-cost VLSI photonics.

2. Theoretical Evaluation of Intrinsic Loss in Ultracompact Microring Resonators

In general, loss in small microring resonators can be attributed to three main sources: bending loss, surface roughness scattering loss, and scattering loss at the coupling junctions between the microring and external bus waveguides. Surface roughness scattering loss is process dependent and can in principle be reduced by optimizing the lithography and etching processes to produce smooth waveguide sidewalls. Coupling junction loss varies inversely with the coupling gap between the bus and ring waveguides and, thus, depends on the coupling strength, which varies according to the application. Bending loss, on the other hand, is an intrinsic loss mechanism which places a theoretical limit on the achievable intrinsic Q factor of a microring resonator with a given bending radius. It is thus of practical interest to investigate the bending loss of microring resonators with very small bending radii to determine the theoretical performance and limit of miniaturization of these devices.

The common approach for determining the bending loss of a curved waveguide is to compute the complex propagation constant of the eigenmode of interest. To accurately determine the loss in very tight bends, we performed rigorous numerical solution of the full-wave vector Helmholtz equation in cylindrical coordinates. For convenience, we adopted the local cylindrical coordinate system (x, y, z), whose transformation from the global cylindrical coordinate system (r, θ, z) for a ring waveguide of radius R with cross section in the r–z plane is given by $r \rightarrow x + R$, $\theta \rightarrow z/R$, $z \rightarrow y$ [9]. The eigenvalue problem for the propagation constant β is then formulated in terms of the H field as

$$\begin{bmatrix} Q_{xx} & Q_{xy} \\ Q_{yx} & Q_{yy} \end{bmatrix} \begin{bmatrix} H_x \\ H_y \end{bmatrix} = \beta^2 \begin{bmatrix} H_x \\ H_y \end{bmatrix} \quad (1)$$

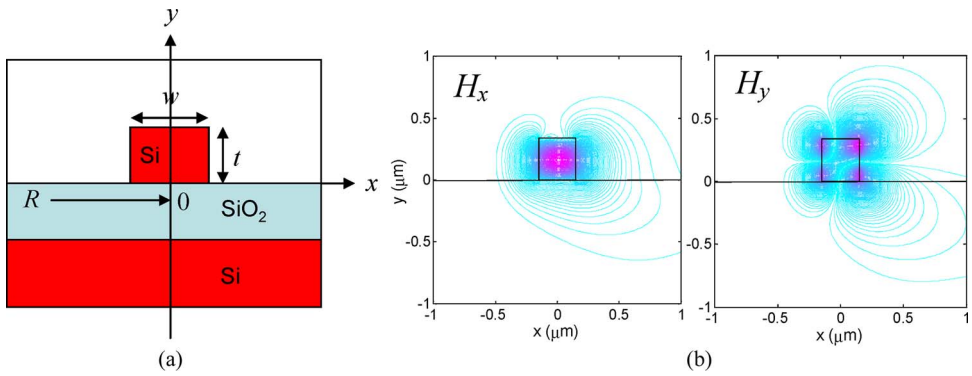

Fig. 1. (a) Cross-sectional view in the local cylindrical coordinates of an SOI microring waveguide. (b) Magnetic field components H_x and H_y of the quasi-TM mode of a 1.0-μm-radius ring waveguide with $t = 340$ nm and $w = 300$ nm.

where the operators Q_{xx}, Q_{xy}, Q_{yx}, and Q_{yy} are expressed in the local cylindrical coordinates as in [10]. For very tight bending radii, significant coupling between H_x and H_y can result so a full vectorial solution must be sought to ensure accurate determination of the eigenvalues. Also, the leaky-mode nature of the tightly bent waveguides necessitates the use of perfectly matched layers (PMLs) [10] on the boundaries of the computational domain.

Although numerous numerical studies of bending loss have been reported for waveguides with fairly large bending radii [10], [12], very few studies have been done for high-index-contrast waveguides with extremely small radii. In [13], numerical analysis of waveguide bends with radius down to 1 μm was performed for a particular waveguide geometry using the Finite-Element method. Here, we performed numerical simulations of SOI microrings with bending radii in the 0.5–1.5-μm range to investigate the systematic dependence of bending loss on the waveguide dimensions and polarization in ultracompact microring resonators. The ring waveguide structure used is shown in Fig. 1(a), which consists of a silicon core of thickness t, width w, and an index of 3.5 residing on a SiO_2 buffer layer of index 1.45. The device was assumed to be air cladded. The eigenmodes of the waveguide were obtained by solving (1) using the Finite-Difference method with a rectangular computational grid of cell size $\Delta x = \Delta y = 10$ nm. A 1-μm-thick PML layer with a quadratic electric conductivity profile with $\sigma_{\max} = 10$ was padded on all four sides of the computational domain to absorb outgoing waves. Typical eigenmode solutions obtained for the magnetic field components H_x and H_y are shown in Fig. 1(b) for the fundamental quasi-TM mode of a 1.0-μm-radius ring waveguide with $t = 340$ nm and $w = 300$ nm. The leaky-wave nature of the mode is evident from the contour field lines showing bending-loss radiation into the SiO_2 substrate.

In Fig. 2(a), we plotted the roundtrip bending losses at 1.55-μm wavelength for the quasi-TE and quasi-TM modes of microrings with 1-μm radius as functions of the waveguide width w. Two values of the waveguide thickness are shown: $t = 340$ nm, which corresponds to the thickness of our fabricated microring structures, and $t = 250$ nm, which is another commonly used SOI waveguide thickness. The right axis of the plot shows the corresponding intrinsic Q factors calculated assuming a group index $n_g = 4.8$ in the ring waveguides. It is seen that for both polarizations, the bending loss decreases roughly exponentially with increasing waveguide width. The ring waveguide with the larger thickness $(t = 340$ nm$)$ also has smaller bending loss. The explicit dependence of the bending loss and intrinsic Q factor on the waveguide thickness t is shown in Fig. 2(b) for fixed waveguide widths of $w = 300$ nm and $w = 450$ nm. A strong exponential dependence of the loss on the thickness is also observed. The plots in Fig. 2(a) and (b) suggest that, in general, microrings with larger waveguide core areas have lower bending loss since they provide stronger mode confinement. Another important result that emerges from the above plots is the strong dependence of the bending loss on the polarization. This dichroic nature of the microrings is a manifestation of the different degrees of modal confinement of the two polarizations, which, in turn, depend on the aspect ratio of the waveguide. For example, in Fig. 2(b), for the waveguide with aspect ratio $t/w = 250/450$ nm (label A), the TM mode exhibits a

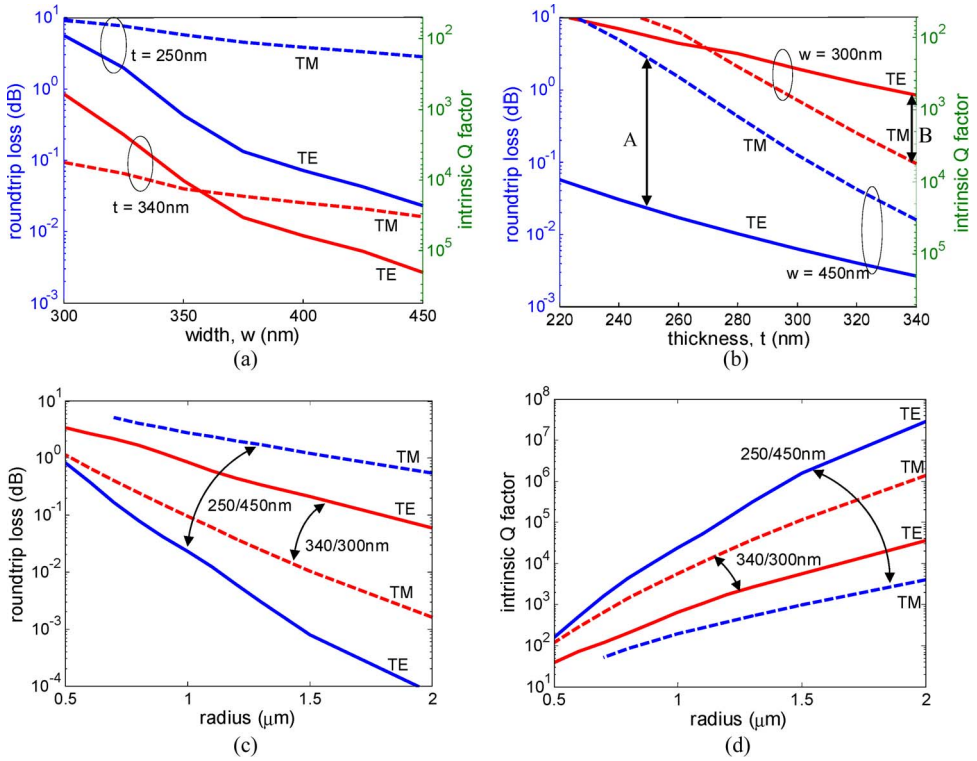

Fig. 2. Dependence of the roundtrip bending loss and intrinsic Q factor at 1.55-μm wavelength of a 1-μm-radius ring waveguide on (a) the waveguide width w and (b) waveguide thickness t. (c) Dependence of the roundtrip bending loss and (d) intrinsic Q factor at 1.55-μm wavelength on the ring radius.

bending loss that is two orders of magnitude larger than the loss experienced by the TE mode. As a result, only the TE mode can resonate in these microrings. This is indeed the mode observed in sharp SOI bends and microrings with similar aspect ratio [7]. On the other hand, for microrings with waveguide aspect ratio $t/w = 340/300$ nm (label B), the TM mode has a much lower bending loss than the TE mode and is thus expected to be the dominant mode of resonance, as observed in our fabricated devices presented in the next section. In general, the plots in Fig. 2(a) and (b) can be used as a guide to design very compact and high-extinction wavelength-selective polarizers based on ultracompact microring resonators by choosing the appropriate aspect ratios for the ring waveguide.

In Fig. 2(c), we examined the roundtrip bending loss at 1.5-μm wavelength as a function of the radius for two waveguide aspect ratios: $t/w = 340/300$ nm (which corresponds to the dimensions of our fabricated microrings) and 250/450 nm (which is similar to structure reported in the literature [7]). The exponential dependence of the roundtrip bending loss on the radius is again evident from the plot. Fig. 2(d) shows the corresponding intrinsic Q factor as a function of the radius for the above two waveguide aspect ratios. It is seen from the plot that for a microring with a radius of 1 μm, the theoretical achievable Q factor is 5600 for the TM mode in the 340/300-nm ring and up to 23 000 for the TE mode in the 250/450-nm ring. Thus, fairly large intrinsic Q factors can be achieved, even with microring resonators with extremely small radii. These results suggest that with suitable choice of the waveguide aspect ratio, it is feasible to realize practical low-loss VLSI photonic circuits based on these ultracompact microring resonators.

3. Fabrication and Experimental Performance of Ultracompact SOI Microring Add–Drop Filters

In order to assess the experimentally achievable performance of microring add–drop filters with very small radii, we fabricated a set of SOI add–drop microrings with radii of 1.5, 1.4, 1.3, 1.1, and 1.0 μm.

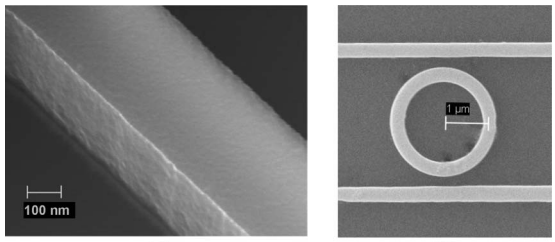

Fig. 3. SEM image of (a) a typical SOI bus waveguide and (b) a silicon add–drop microring resonator with 1.0-μm radius.

The devices were realized on an SOI wafer consisting of a 340-nm Si layer on a 1-μm buried oxide layer. The waveguide width was 300 nm and the coupling gaps between the bus and ring waveguides were fixed at 200 nm. In the fabrication process, the structures were first written on a 100-nm-thick layer of the positive resist poly-methyl-methacrylate (PMMA) using a Raith 150 E-beam lithography (EBL) system. The chip was next developed with a MIBK : IPA (1 : 3) high-resolution developer solution. A precision anisotropic etch recipe based on fluorine chemistry, developed on an inductively-coupled-plasma reactive-ion-etching (ICPRIE) system, was used to transfer the resist pattern through the 340-nm-deep Si layer. Finally, the remaining PMMA was removed and the chip was cleaved to expose the waveguide facets for butt-coupling with a fiber. Fig. 3(a) is a scanning electron microscope (SEM) image of a typical sidewall of the bus waveguides, showing the overall surface roughness achieved through the above fabrication process. Fig. 3(b) shows an SEM image of the fabricated microring with a 1.0-μm radius. In all the devices the ring waveguide widths were measured to be 310 $\pm$ 5 nm, and the coupling gaps between the microring and the bus waveguides were 200 $\pm$ 5 nm.

Spectral measurements of the devices were taken using an experimental setup consisting of a 1510–1630-nm continuous-wave tunable laser coupled to the input waveguide via a tapered-lensed fiber. The polarization state of the laser was adjusted to the transverse magnetic (TM) mode using a fiber polarization controller. Only TM measurements are presented in this work since our microring resonators (with aspect ratio $t/w = 340/300$ nm) predominantly supported only the TM modes, as predicted by the simulation results in Fig. 2. This is also confirmed by separate spectral scans we performed with TE polarized light, which showed no observable TE resonance peaks. The output light from the device was collected by another lensed fiber and fed into an InGaAs photodetector. For each device on the chip, there was a 1.5-mm-long input and output waveguide leading from the edge of the chip to the device. To improve the coupling efficiency to the lensed fiber, the input and output waveguide widths were flared out to 2 μm at each of the facets, which were not coated with an antireflection coating. From repeated alignments and measurements, we found that we could achieve the coupled powers to within $\pm$0.1 dB so that the effect of mismatch in the input and output couplings was negligible.

Fig. 4 shows the measured spectral responses at the through port and drop port of the fabricated microrings with different radii. The mode number m associated with each resonance peak is also labeled in the plots. It is observed that in general, the microrings exhibited broader resonances at longer wavelengths, which signify higher loss and stronger coupling. At long wavelengths, the waveguide modes are less confined and thus have larger bending loss, which is a trend that has been confirmed by the simulation results in [13]. As we show in Fig. 5(a), the coupling loss and coupling efficiency between a bent and straight waveguide also increase with wavelength, which also lead to broadening of the microring resonance width. From the spectral measurements, the 3-dB bandwidth, FSR, and peak insertion loss of each device were obtained and the results tabulated in Table 1. The insertion loss of the devices varies between 1 and 2 dB, with the excessive loss observed in the 1.1-μm-radius microring most likely due to fabrication anomaly since it is substantially worse than the other devices, including the smaller 1.0-μm-radius microring. Notably, for the smallest add–drop microring filter with 1.0-μm radius, we obtained an insertion loss of only $\sim$1 dB with an extremely

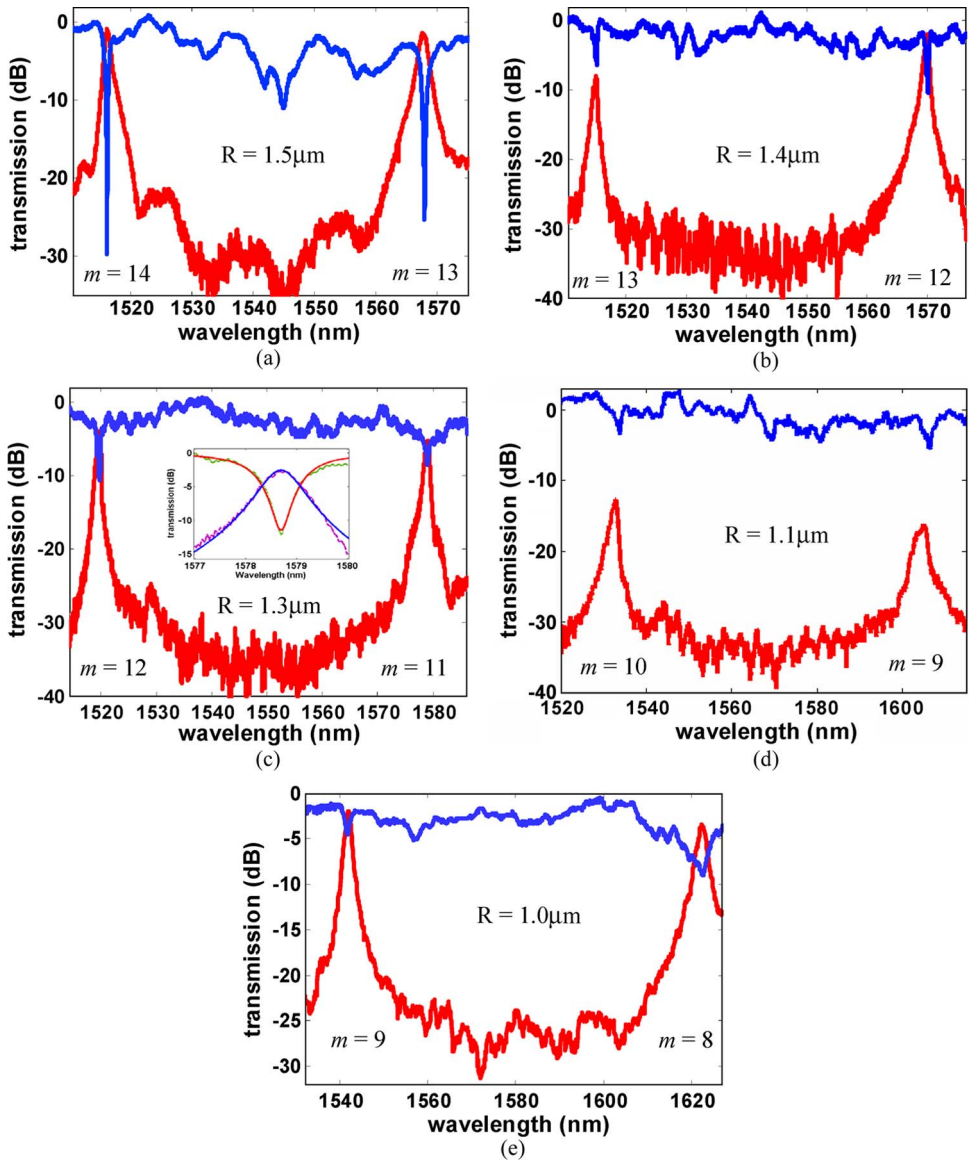

Fig. 4. Measured spectral responses at the drop port (red) and through port (blue) of microring resonators with radius of (a) 1.5 μm, (b) 1.4 μm, (c) 1.3 μm, (d) 1.1 μm, (e) 1.0 μm. The number m indicates the cavity mode number. The inset in (c) shows a theoretical curve fit of the resonance spectrum at 1580 nm of the 1.3-μm microring.

wide FSR of 80.5 nm, which spans almost both the C and L bands. These results suggest that the device has potential application as WDM add–drop filters with very wide tuning range.

By performing curve fitting of the measured spectral responses, we could also extract the ring-to-bus coupling coefficient and the roundtrip loss of each microring [14]. A typical curve fit is shown in the inset of Fig. 4(c) for the 1.3-μm-radius microring at the 1580-nm resonant wavelength. The good fit between the computed and measured spectral responses allowed us to determine the device parameters fairly accurately. The results for the extracted coupling coefficient κ^2 and the total roundtrip loss for each device are also summarized in Table 1.

The extracted roundtrip loss values in Table 1 represent the total roundtrip loss, which includes the bending loss, coupling junction loss, and surface roughness scattering loss. To assess the loss contribution due to coupling junction scattering, we performed 3-D-finite difference time-domain simulations of the coupling junctions between a straight waveguide and bent waveguides of radii

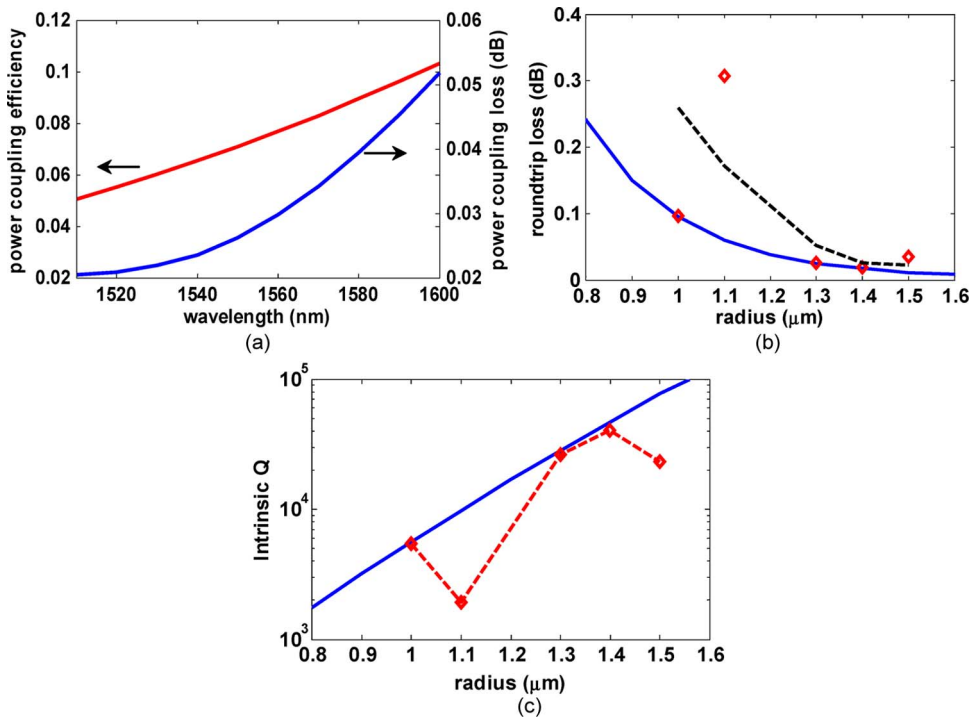

Fig. 5. (a) Theoretical power coupling efficiency (red) and power coupling loss per junction (blue) as a function of wavelength for a coupling junction between a 1.3-μm-radius bent waveguide and a straight waveguide. (b) Theoretical roundtrip bending loss (blue line), roundtrip coupling junction loss (dashed black line), and measured intrinsic roundtrip loss (red diamonds) of microring resonators as function of radius. (c) Experimental values (red diamonds) and theoretical limit (blue line) of intrinsic *Q* factors of microring resonators as function of radius.

TABLE 1

Measured and extracted device parameters for SOI microring add–drop filters with radii between 1.0–1.5 μm

	Add-drop filter characteristics			Microring resonator characteristics		
Radius (μm)	FSR (nm)	Bandwidth (nm)	Insertion loss (±0.2dB)	Coupling coefficient κ^2	Total roundtrip loss (dB)	Intrinsic *Q* factor
1.5	52	1.2	0.95	0.076	0.11	23,280
1.4	55	1.0	1.9	0.034	0.045	40,280
1.3	59.6	1.0	2.1	0.070	0.079	26,430
1.1	71.7	3.0	15	0.047	0.52	1,920
1.0	80.5	3.3	0.85	0.073	0.35	5,460

from 1.0 to 1.5 μm. The coupling gap was fixed at 200 nm. First, we examined the wavelength dependence of the power-coupling efficiency and power-coupling loss by plotting them as functions of wavelength in Fig. 5(a) for a coupling junction between a straight waveguide and a 1.3-μm-radius bent waveguide. It is seen that both the coupling efficiency and coupling loss increase with wavelength. This is due to the fact that at longer wavelengths the modes in the waveguides become less confined so that there is more mode overlap between the waveguides leading to stronger coupling, as well as more pronounced scattering at the coupling junction. As mentioned above, the increase in the coupling efficiency and coupling loss both contribute to a slight broadening of the microring resonance bandwidth at longer wavelengths. Next, we plotted in Fig. 5(b) the roundtrip coupling loss due to scattering from two coupling junctions in an add–drop microring filter as a

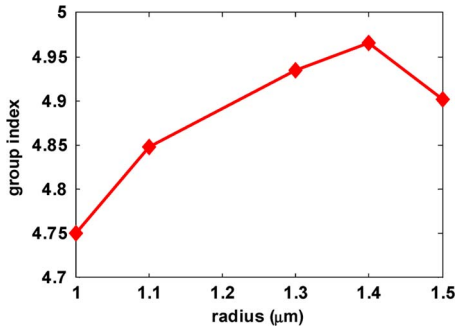

Fig. 6. Measured group index of ultracompact microring resonators as function of the radius.

function of the microring radius (black dashed line). It is seen that the coupling loss varies inversely with the radius, which is expected since tighter bends represent more abrupt changes in the coupling junction. More significantly, we note that compared to the theoretical roundtrip bending loss, which is shown by the blue line in Fig. 5(b), the coupling junction loss is actually larger and is in fact the dominant source of loss for microrings with radius below 1.5 μm. After subtracting the coupling junction loss from the measured total roundtrip loss values in Table 1, we plotted the results in Fig. 5(b) (red diamonds), which can be regarded as the experimental intrinsic loss of the fabricated microrings. The results are seen to agree fairly well with the theoretical bending loss values (except for the 1.1-μm-radius microring), implying that loss due to surface roughness scattering plays a much less significant role than bending loss and coupling loss in these ultracompact microrings. We next computed the intrinsic Q factors of the fabricated devices using the experimental intrinsic loss values in Fig. 5(b). The results are shown in Table 1 and are also plotted in Fig. 5(c) (red diamonds). For comparison, the theoretical Q factors due to the bending loss alone, which represent the theoretical limit of achievable intrinsic Q values, are also plotted in Fig. 5(c) (blue line). The close agreement between the experimental and theoretical values shows that the intrinsic Q factors of our fabricated microring resonators (in particular, the 1.0- 1.3-, and 1.4-μm devices) are very close to the theoretically achievable limit.

From the measured FSR values of the microring resonators, we also computed the group index n_g of the SOI microrings using the relation FSR $= \lambda^2/2\pi R n_g$, where $\lambda = 1550$ nm. The results are plotted in Fig. 6 as a function of the microring radius, which shows that the TM group index of the microring decreases from $\sim$4.95 for $R = 1.4-1.5$ μm to 4.75 for $R = 1.0$ μm. The decrease in n_g with decreasing R can be explained by the fact that as R decreases, the mode in the microring waveguide becomes more loosely bound so the strong dispersive effect normally associated with the silicon waveguide core becomes less dominant. We note that the group index values of $\sim$4.95 obtained for microrings with larger radii $(R > 1.3$ μm$)$ are comparable to the value of $n_g \sim 5$ obtained in [15] for relatively straight SOI waveguides at wavelengths far from the TM mode cutoff. Finally, the drop in the group index of the 1.5-μm device [as well as its Q factor in Fig. 5(c)] is most likely due to proximity effect in lithography process, which may have caused a slight narrowing of the coupling gap compared with the other devices.

4. Conclusion

We presented rigorous numerical analyses of the bending loss, coupling loss, and intrinsic Q factors in extremely compact SOI add–drop microring filters to explore their limit of miniaturization. Theoretical results showed that the bending loss depends strongly on the aspect ratio of the microring waveguide as well as the polarization. With a suitable choice of the waveguide aspect ratio, theoretical intrinsic Q factors in the order of 10^4 can be achieved in microring resonators with bending radius as small as 1 μm for either polarization. We also showed that for ultracompact microring add–drop filters, the dominant source of loss comes from scattering from the two bus-to-ring coupling junctions rather than the bending loss. This finding is significant because it offers

possible avenues for further improving the performance of ultracompact microring add–drop filters by optimizing the coupling junctions to reduce scattering loss. For example, a possible approach is to use curved bus waveguides in order to reduce the curvature mismatch between the bus and microring waveguides, leading to reduced scattering. Another approach as suggested in [7] is to reduce the bus waveguide width to reduce loss due to coupling into higher order modes. By accounting for the extrinsic loss due to coupling junction scattering, we showed that our fabricated microring resonators exhibited intrinsic *Q* factors that are very close to the theoretically achievable limit. These devices also showed promising add–drop filter performances in terms of low insertion loss, wide FSRs, and ultracompact sizes, suggesting that it is feasible to achieve practical device performance with extremely miniaturized microring resonators for very dense integration of Silicon photonic devices.

Acknowledgment

The authors wish to thank S. Buswell for his assistance with the SEM.

References

[1] S. Xiao, M. H. Khan, H. Shen, and M. Qi, "Silicon-on-insulator microring add-drop filters with free spectral ranges over 30 nm," *J. Lightw. Technol.*, vol. 26, no. 2, pp. 228–236, Jan. 2008.
[2] F. Xia, M. Rooks, L. Sekaric, and Y. Vlasov, "Ultra-compact high order ring resonator filters using submicron silicon photonic wires for on-chip optical interconnects," *Opt. Express*, vol. 15, no. 19, pp. 11 934–11 941, Sep. 2007.
[3] Q. Xu, B. Schmidt, S. Pradhan, and M. Lipson, "Micrometer-scale silicon electro-optic modulator," *Nature*, vol. 435, pp. 325–327, 2005.
[4] F. Xia, L. Sekaric, and Y. A. Vlasov, "Ultra-compact optical buffers on a silicon chip," *Nat. Photon.*, vol. 1, no. 1, pp. 65–71, Jan. 2007.
[5] A. M. Prabhu, A. Tsay, Z. Han, and V. Van, "Ultracompact SOI microring add–drop filter with wide bandwidth and wide FSR," *IEEE Photon. Technol. Lett.*, vol. 21, no. 10, pp. 651–653, May 2009.
[6] M. S. Nawrocka, T. Liu, X. Wang, and R. R. Panepucci, "Tunable silicon microring resonator with wide free spectral range," *Appl. Phys. Lett.*, vol. 89, no. 7, p. 071 110, Aug. 2006.
[7] Q. Xu, D. Fattal, and R. G. Beausoleil, "1.5-μm-radius high-Q silicon microring resonators," *Opt. Express*, vol. 16, pp. 4309–4315, 2008.
[8] W. Bogaerts, D. Taillaert, B. Luyssaert, P. Dumon, J. Van Campenhout, P. Bienstman, D. Van Thourhout, R. Baets, V. Wiaux, and S. Beckx, "Basic structures for photonic integrated circuits in silicon-on-insulator," *Opt. Express*, vol. 12, no. 8, pp. 1583–1591, Apr. 2004.
[9] M. Rivera, "A finite difference BPM analysis of bent dielectric waveguides," *J. Lightw. Technol.*, vol. 13, no. 2, pp. 233–238, Feb. 1995.
[10] J. Xiao, H. Ma, N. Bai, X. Liu, and X. Sun, "Full-vectorial analysis of bending waveguides using finite difference method based on H-fields in cylindrical coordinate systems," *Opt. Commun.*, vol. 282, no. 13, pp. 2511–2515, Jul. 2009.
[11] W. C. Chew and W. H. Weedon, "A 3D perfectly matched medium from modified Maxwell's equations with stretched coordinates," *Microw. Opt. Technol. Lett.*, vol. 7, no. 13, pp. 599–604, Sep. 1994.
[12] N.-N. Feng, G.-R. Zhou, C. Xu, and W.-P. Huang, "Computation of full-vector modes for bending waveguide using cylindrical perfectly matched layers," *J. Lightw. Technol.*, vol. 20, no. 11, pp. 1976–1980, Nov. 2002.
[13] K. Kakihara, N. Kono, K. Saitoh, and M. Koshiba, "Full-vectorial finite element method in a cylindrical coordinate system for loss analysis of photonic wire bends," *Opt. Express*, vol. 14, no. 23, pp. 11 128–11 141, Nov. 2006.
[14] V. Van, P. P. Absil, J. V. Hryniewicz, and P.-T. Ho, "Propagation loss in single-mode GaAs-AlGaAs microring resonators: Measurement and model," *J. Lightw. Technol.*, vol. 19, no. 11, pp. 1734–1739, Nov. 2001.
[15] E. Dulkeith, F. Xia, L. Schares, W. M. J. Green, and Y. A. Vlasov, "Group index and group velocity dispersion in silicon-on-insulator photonic wires," *Opt. Express*, vol. 14, no. 9, pp. 3853–3863, May 2006.